Applied Surface Science 407 (2017) 398–404

Contents lists available at ScienceDirect

Applied Surface Science

journal homepage: www.elsevier.com/locate/apsusc

Full Length Article

High performance silicon-organic hybrid solar cells via improving conductivity of PEDOT:PSS with reduced graphene oxide

Xinyu Jiang[a], Zilei Wang[a], Wenhui Han[a], Qiming Liu[a], Shuqi Lu[a], Yuxiang Wen[a], Juan Hou[c], Fei Huang[b], Shanglong Peng[a,*], Deyan He[a], Guozhong Cao[b,*]

[a] School of Physical Science and Technology, Key Laboratory for Magnetism and Magnetic Materials of the Ministry of Education, Lanzhou University, Lanzhou 730000, PR China
[b] Department of Materials Science and Engineering, University of Washington, Seattle, WA 98195-2120, United States
[c] School of Science, Key Laboratory of Ecophysics, Shihezi University, Xinjiang 832003, PR China

ARTICLE INFO

Article history:
Received 1 January 2017
Received in revised form 12 February 2017
Accepted 21 February 2017
Available online 24 February 2017

Keywords:
Hybrid solar cells
Power conversion efficiency
Reduced graphene oxide
Conducting polymers

ABSTRACT

The optical and electrical properties of PEDOT:PSS organic layer play a very important role in determining the power conversion efficiency (PCE) of Si-organic hybrid solar cells (HSCs). In the present study, properties of PEDOT:PSS thin films with reduced graphene oxide (rGO) and their impacts on the performances of the resultant Si-organic HSCs have been systematically investigated. The electrical conductivity of PEDOT:PSS improved 35% when rGO was added to PEDOT:PSS, and the fabricated HSCs with 2 mg/ml rGO addition yielded an PCE of 11.95% with a J_{sc} of 31.94 mAcm^{-2}, a V_{oc} of 579 mV and a *FF* of 0.648. However, excess rGO would deteriorate the solar cells performances and it might create additional defects and prevent carriers being collected. The Raman spectroscopy, sheet resistance and EQE analyses with rGO suggested that the interaction between the conductive rGO flakes and the aromatic PEDOT most probably not only provide additional charge transport pathways in hole transport layer to improve carrier mobility leading to a higher carrier collection efficiency, but also suppress the electron recombination at the junction interface. In addition, the rGO serve as an antireflection coating to reduce the reflectance of PEDOT:PSS thin film leading to further enhanced performances of solar cells.

1. Introduction

The Si-based solar cells play an important role in photovoltaic market for its mature manufacturing process and abundant raw materials in the world [1]. But the purification and fabrication processes occupy a vast majority of the total cost. Although the Si photovoltaic industry is refining on several thin-wafer or thin-film technologies to reduce the material cost, there are very limited solutions to cut down the fabrication processes significantly [2]. In recent years, the emergence of Si-organic HSCs offers a practical means to reduce cost by adopting low-temperature, scalable, and soluble processes of conjugated polymers to form heterojunctions with an n-type crystalline Si at the interface [3]. In particular, solar cells made of a p-type conjugated polymers, such as poly(3,4-ethylenedioxythiophene):poly(stryrenesulfonate) (PEDOT:PSS), on a n-type Si substrate are gaining strong interest mainly due to the simple fabrication processes, less pollution and easier commercialization [4,5]. For this type Si-organic HSCs, incident photons are harvested by Si generating electron-hole pairs instead of organics, depletion layer could be formed in n-type crystalline Si when p-type organic layer is deposited on the surface of Si. Here, organic layer can block electrons and let hole pass, and act as surface passivation, charge extraction, optical window and light antireflection for Si-organic HSCs [6–8]. Zielke et al. demonstrated that the PCE of HSCs up to 20% could be achieved by optimizing the device structure and organic layer selection [9]. And the PCE is fundamentally determined by optical absorption in the Si absorber, carrier separation and recombination at the interface, charge transport path through organic layer, as well as top and bottom electrode configurations [10–12]. Over the past few years, several schemes have been proposed to improve the performance of Si-organic HSCs, such as Si textures for light harvesting, surfactant-treated conductive polymer for high conductivity, organic interface passivation [8,13,14]. Recently, Yu, et al. have utilized a small organic molecule 1,1-bis[(di-4-tolylamino) phenyl] cyclohexane layer into the interface between Si and PEDOT:PSS to suppress the short circuit current density (J_0), leading to a boosted

* Corresponding authors.
E-mail addresses: pengshl@lzu.edu.cn (S. Peng), gzcao@u.washington.edu (G. Cao).

http://dx.doi.org/10.1016/j.apsusc.2017.02.193
0169-4332/

the open-circuit voltage (V_{oc}) and fill factor (*FF*) [4]. Thomas, et al. have demonstrated that adhesion between organic layer and Si was dramatically improved by adding different surfactants into PEDOT:PSS, resulting in a PCE over 13% [15]. And Liu, et al. have utilized p-Toluenesulfonic acid in PEDOT:PSS to increase its conductivity up to 2000 S cm^{-1}, a PCE of 15.5% was achieved with an antireflection layer of TiO_2 on Si-organic HSCs [16]. Moreover, much effort to suppress the light reflection and enhance the photo-generated carrier collection efficiency has been made for the purpose of optical and electrical concurrent improvement via nanostructured solar cells [17]. However, there is still a large gap in efficiency between hybrid and conventional Si solar cells, impeding their development to becoming cost-effective devices.

PEDOT:PSS is a polymer electrolyte consisting of positively charged conjugated PEDOT and negatively charged saturated PSS. PSS is a polymer dispersant, which helps disperse and stabilize PEDOT in water and other solvents. PEDOT:PSS is the most successful conducting polymer in terms of practical applications. PEDOT:PSS thin film exhibits high transparency in the visible range, high mechanical flexibility, excellent thermal stability, a high work function (5.0–5.2 eV) and relatively facile process ability, for which it have recently proven to be one of the most promising candidates as transparent conductive layers and hole transport layers in solar cells and electroluminescence devices [18]. The conductivity can be increased to 1000 S cm^{-1} by adding polar solvents, such as methanol (MeOH), ethylene glycol (EG), or MeOH/EG co-solvents [16,19]. A small addition of zonyl fluoro-surfactant also improved the uniformity of spin-coated PEDOT:PSS on hydrophobic H-terminated c-Si [20]. However, comparing to the n type Si wafer, the poor conductivity of PEDOT:PSS hinders the carriers transport for the Si-organic HSCs. Therefore, more efforts have been put forward to further help improve the conductivity of PEDOT:PSS, which is the main issue weakening the charge collection capability and a low photovoltaic properties.

Graphene has attracted huge amount of attention as a highly promising material for many applications in nano-electronics, solar cells, batteries and supercapacitors because of large specific surface area, fascinating electrical conductivity and high mechanical strength [21–23]. Recently, graphene has been combined with PEDOT:PSS using different methods for various electronic applications [24,25]. And a double-layered graphene/PEDOT:PSS thin film was prepared with optical and electrical properties for large-area flexible optoelectronic devices [26]. Also, graphene/PEDOT:PSS thin film was fabricated as the counter electrodes to improve the performances of dye-sensitized solar cells [27–29]. And Tang et al. exhibited a the heterojunction devices c-Si/PEDOT:PSS: graphene oxide (GO) maximum efficiency of 10.3% [30].

In the present investigation, a small amount of rGO via ultrasonic cell disruptor treatment blended with PEDOT:PSS as hole transport layer to improve the performances of Si-organic HSCs. It can be found that the introduction of rGO to PEDOT:PSS can effectively improve the J_{sc}, V_{oc} and *FF* of Si-organic HSCs. And the PCE of Si-organic HSCs with the addition of 2 mg/ml rGO reached to 11.95% with V_{oc} of 0.579 V, J_{sc} of 31.94 mAcm^{-2} and *FF* of 0.648, an almost 27.8% enhancement compared to the pristine HSCs. And the influences of morphology, optical and electrical properties of the PEDOT:PSS/rGO thin films on the performances of HSCs have been studied and discussed.

2. Experiment

2.1. Preparation of n-type Si wafer

300 μm thick, one-side polished n-type (100)-oriented crystalline Si wafers with a resistivity of 1–5 Ω cm were used for experiments. It was ultrasonically cleaned in acetone, ethanol and deionized water for 15 min, followed by immersing into 5% HF solution for 3 min to remove the oxide layer. Then, the samples were dried by a steam of N_2.

2.2. Preparation of PEDOT:PSS/rGO dispersion

The GO was annealed at 300 °C for 2 h in a mixed gas of hydrogen and argon (the molar ratio of H_2 to Ar was 3:10). And the GO was reduced into rGO flakes. Then, rGO was grinded in the mortar for 1 h to get the uniform particles. Next the rGO was added into 1 ml EG solution with concentration of 1 mg/ml, 2 mg/ml and 3 mg/ml, respectively. The mixture was put into anultrasonic cleaner for 30 min to get the dispersion. Then the obtained dispersion was kept for 1 h using ultrasonic cell disruptor to get uniform and small rGO flakes (The comparison sample without ultrasonic cell disruptor treatment). After ultrasonic procedure, PEDOT:PSS (Clevios™ pH 1000) dispersion was mixed with the 7 wt% EG (added with rGO) solution. And the mixture was processed by a magnetic stirring then ultrasonic each for 1 h. To improve the wettability of PEDOT:PSS on Si wafer, 0.1 wt% zonyl surfactant was also added prior to spin-coating.

2.3. Fabrication of Si-organic hybrid solar cells

The obtained PEDOT:PSS/rGO dispersion was spin-coated onto the cleaned Si wafer using a spin rate of 3000 rpm for 40 s followed annealed at 140 °C for 20 min in air. Subsequently, the top electrode grid was prepared by sliver paste using a shadow mask. Finally, the InGa eutectic layer was used to form an ohmic contact at the Si backsides. An overview of the fabrication process for Si-organic HSCs is shown in Fig. 1.

2.4. Material and device characterization

The structure and morphology of the samples were measured using a X-ray photoelectron spectroscopy (XPS, Kratos AXIS Ultra DLD instrument with an AL K probe beam), X-ray diffraction (XRD, X'Pert Pro Philips, Cu K radiation, 0.154056 nm), Raman spectra (Jobin-Yvon LabRAM HR800 UV, YAG 532 nm), field-emission scanning electron microscopy (FE-SEM, Hitachi, S-4800), and transmission electron microscopy (TEM, FEI, Tecnai G2 F30). The conductivity of the samples was carried out using the four-point probe method in a Van der Pauw configuration (RTS-9 dual four-probe electrical measurement tester). The current density versus voltage (J-V) characteristics of the solar cell were measured using a solar cell characterization system (PV measurement IV5) under AM 1.5G conditions at an illumination intensity of 100 mW/cm^2, calibrated by a standard Si solar cell (PVM937, Newport). The EQE and reflectance characteristics of the device were measured with Zolix QE system.

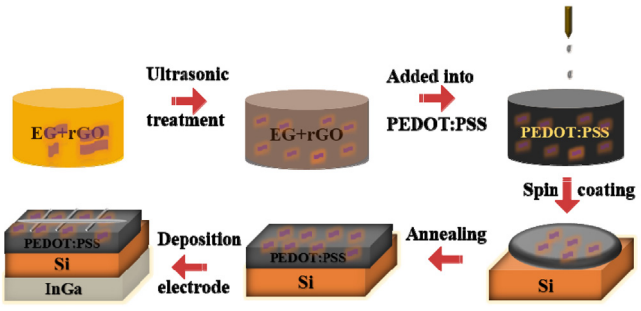

Fig. 1. An overview of the fabrication process for Si-PEDOT:PSS hybrid solar cells.

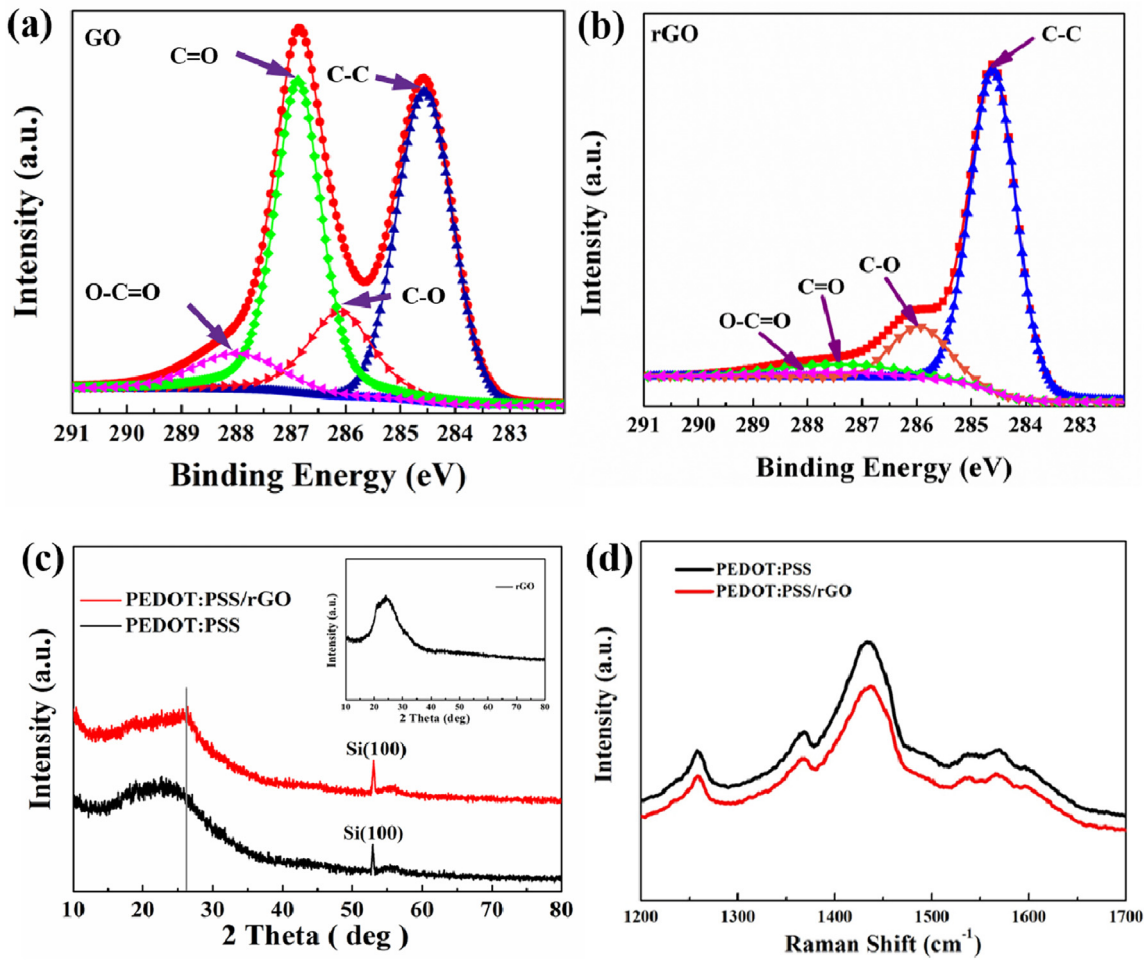

Fig. 2. C1s XPS spectra of (a) GO and (b) rGO. (c). XRD patterns of PEDOT:PSS and PEDOT:PSS/rGO. (Inset is the pattern of rGO flakes) (d) Raman spectra of PEDOT:PSS and PEDOT:PSS/rGO.

3. Results and discussion

XPS measurement was carried out to investigate the formation of rGO which is a core material for improvement of the device performances. The C1s spectra of GO and rGO are presented in Fig. 2a and b, respectively. Differences between the C1s spectra of GO and rGO are evident in shape and peak identity. And It can be seen that a significantly larger proportion of oxygen in GO existed in the form of C—O functionalities. However, according to C1s spectra analysis of rGO in Fig. 2b, after the H_2 thermal reduction of GO, the peaks of oxygen-containing groups at 286.0 eV (C—O), 286.9 eV (C=O) and 288.0 eV (O—C=O) decreased to a different degree [31,32]. The proportion of C=O and O—C=O groups dropped greatly, indicating that most of the oxygen-containing functional groups were removed by H_2 thermal reduction. Besides, the XRD pattern of the GO and rGO also shown in Fig. S1, suggesting that GO was turned into rGO after H_2 reduction at 300 °C too.

The measured of XRD for the PEDOT:PSS and PEDOT:PSS/rGO samples shown in Fig. 2c, and it did not yield any peaks characteristic for PEDOT:PSS thin film except the low angle peak at about 24°, indicating the amorphous nature of the polymeric material. The rGO flakes shows a broad peak at 25.8° (inset in Fig. 2c), after rGO flakes dispersion in PEDOT:PSS solution, the peak could be found in the XRD pattern of the composite films indicating the good dispersion of rGO in composite [33]. And the diffraction at 53.4° corresponds to the (100) plane of the Si substrate.

Raman spectra measurements was used to probe the conformational changes of PEDOT:PSS with rGO addition, as shown in Fig. 2d. For the PEDOT:PSS and PEDOT:PSS/rGO, the five typical bands were indicated as C—C inter-ring stretching (1258 cm^{-1}), single C—C bond stretching (1365 cm^{-1}), C=C symmetric stretching (1433 cm^{-1}), C=C asymmetric stretching (1530 cm^{-1}) and C=C antisymmetric stretching (1569 cm^{-1}) [34]. Compared with the spectra of PEDOT:PSS, the peaks of PEDOT:PSS/rGO are slightly shifted (for example, from 1433 cm^{-1} to 1438 cm^{-1} in case of C=C symmetrical stretching) owing to the strong π-π interactions of aromatic structures in PEDOT:PSS and electron-rich rGO [35]. In addition, the use of XPS to analyze the binding energy clarifies the nature of the binding between rGO and PEDOT:PSS as shown in Fig. S2. Moreover, the peak of C—C peak in PEDOT:PSS and PEDOT:PSS/rGO were slightly shifted from 284.60 to 284.65 eV as shown in Fig. S2c. The shifted peak location also reveals the strong π-π interaction between rGO and the aromatic structure of PEDOT and PSS component [35].

Fig. 3a and b show the cross-section SEM images of PEDOT:PSS and PEDOT:PSS/rGO (with 2 mg/ml rGO) thin films. It can be seen that the inthickness of thin film is ~70 nm and has no significant change after rGO addition. Fig. 3c is the TEM image of rGO flakes after sonication, and some wrinkles and folds with the high specific surface area can be clearly seen, which can benefits the contact area between the PEDOT:PSS polymer and c-Si [36]. Fig. 3d presents the TEM image of PEDOT:PSS/rGO thin film. It can be found that the

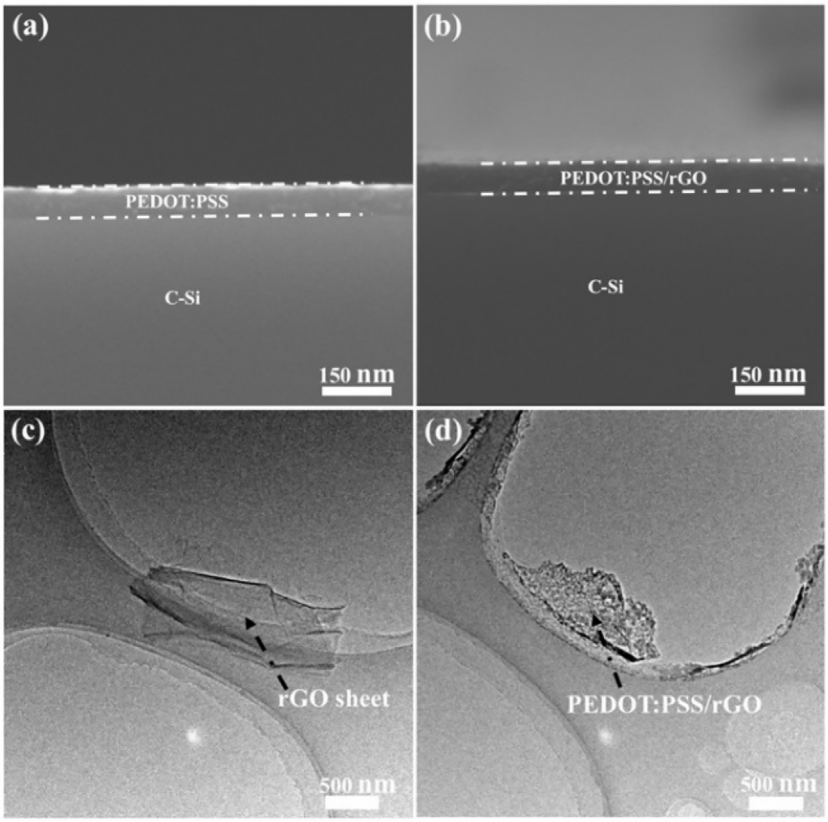

Fig. 3. The cross-sectional SEM images of PEDOT:PSS (a) and PEDOTPSS/rGO thin film (b). The TEM images of rGO flakes (c) and PEDOT:PSS/rGO thin films (d). (all the film was coated on Si substrate at a spin rate of 3000 rpm for 40 s and annealed at 140 °C for 20 min).

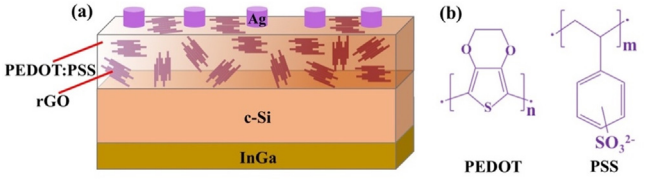

Fig. 4. Schematic diagram of the Si-organic hybrid solar cells (a). Molecular structure of PEDOT and PSS (b).

PEDOT:PSS is covered on the surface of rGO sheets, indicating that stable PEDOT:PSS forms a tightly coated layer on the surface of rGO, just like a blanket which connect each segregated agglomerated PEDOT particles together, and it can provide additional charge transport pathways, and thus deliver a superior capacity of charge carrier-transport property in the conductive composite of PEDOT:PSS/rGO [35,36].

The schematic diagram of the device structure based on n-Si and PEDOT:PSS with rGO homogeneously dispersed is depicted in Fig. 4a. Molecular structures of PEDOT and PSS used in this study is shown in Fig. 4b. It is known that PEDOT:PSS consists of hydrophobic conductive PEDOT coordinated by hydrophilic, insulating PSS chains via ionic chemical bonds. After sequential device fabrication processes, the Si-organic HSCs were made with different amounts of rGO addition (1 mg/ml, 2 mg/ml, 3 mg/ml mixed in EG solution then added 7wt% mixture into PEDOT:PSS solution). And the pristine device was made from PEDOT:PSS mixed with 7wt% EG solution for comparison.

To investigate the effect of the conductivity of PEDOT:PSS thin films on the performances of HSCs, we have measured the sheet resistance of PEDOT:PSS thin films as a function of the rGO concentration. For each type of film, three different samples were

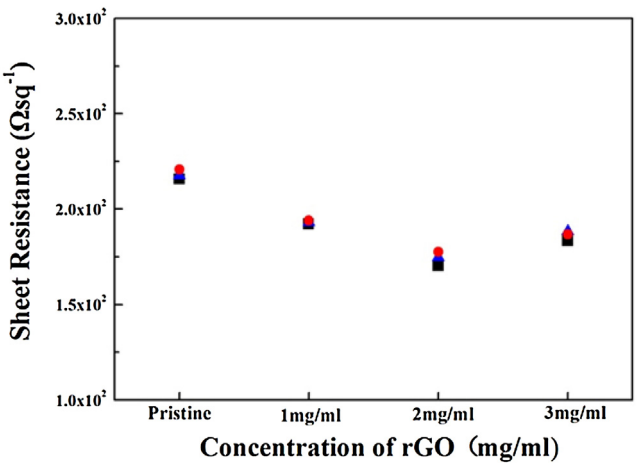

Fig. 5. The sheet resistance of PEDOT:PSS thin films as a function of the rGO content. (blue diamonds represent the average value, red circles represent the maximum value and black squares represent the minimum value, each sample was tested for 5 times. all the film layer on glass substrate was coated at a spin rate 3000 rpm for 40 s and annealed at 140 °C for 20 min. the samples were ~70 nm in thickness). (For interpretation of the references to colour in this figure legend, the reader is referred to the web version of this article.)

measured, and the conductivity was evaluated using $\sigma = 1/R_{sh}d$, where R_{sh} is the sheet resistance determined from four-point probe measurements, and d is the film thickness obtained from SEM measurements. It can be seen in Fig. 5 that the sheet resistance of the PEDOT:PSS thin films decreased approximately 35%, from 225 Ω/sq (pristine) to 170 Ω/sq (2 mg/ml rGO addition), then increased to 186 Ω/sq (3 mg/ml rGO addition). In view of the excellent conduc-

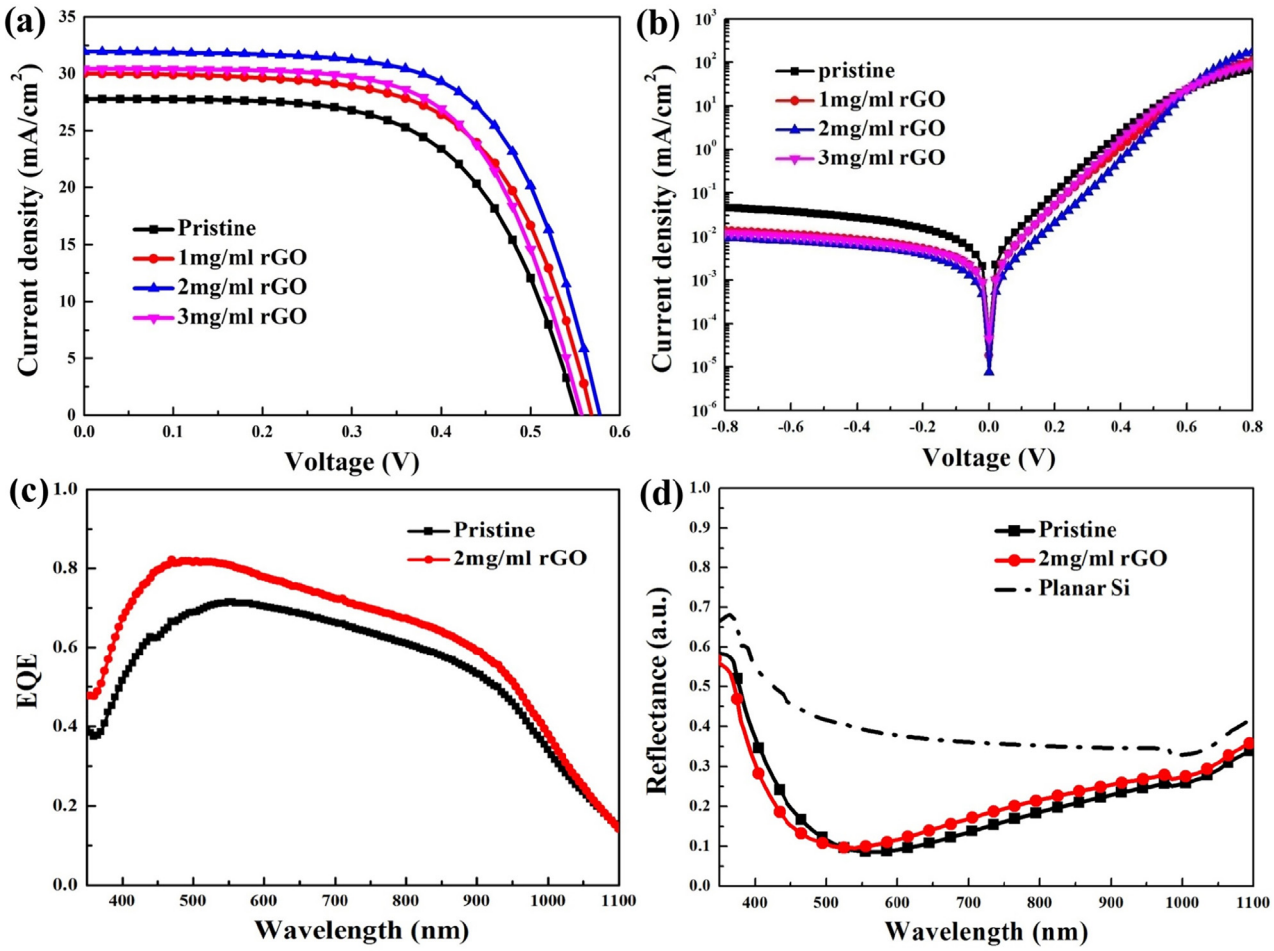

Fig. 6. J-V curves of the Si-organic hybrid solar cells under illumination of AM 1.5G light (a) and in dark (b). EQE of Si-organic hybrid solar cells without and with 2 mg/ml rGO addition (c). The optical reflectance of Si wafer, PEDOT:PSS/c-Si and PEDOT:PSS(rGO)/c-Si composite thin films (d).

Table 1
Performance details of Si-organic hybrid solar cells with different rGO addition.

Devices	J_{sc} (mA/cm^2)	V_{oc} (V)	*FF* (%)	η (%)	*Rs* (Ωcm^2)
Pristine	27.78	0.552	60.98	9.35	4.22
1 mg/ml	30.01	0.568	62.42	10.65	3.72
2 mg/ml	31.94	0.579	64.75	11.95	3.02
3 mg/ml	30.41	0.558	63.53	10.77	3.49

tivity of rGO, the electrical conductivity of PEDOT:PSS thin films has been effectively improved by the rGO addition, which in turn lead to reduced leakage current density as shown in Fig. 6b. Therefore, the addition of an appropriate amount of rGO enhanced the electrical conductivity of PEDOT:PSS thin films, thus the device performances also were improved significantly.

In order to investigate the effect of addition of rGO to PEDOT:PSS on the performances of Si-organic HSCs, the illuminated and dark J-V curves of the Ag/c-Si/PEDOT:PSS/InGa heterojunction solar cells without and with different concentration of rGO addition were respectively taken as depicted in Fig. 6a and b. The HSCs parameters V_{oc},J_{sc}, *FF*, η and the calculated series resistance (R_s) are summarized in Table 1. The Pristine device based on Ag/c-Si/PEDOT:PSS/InGa structure yielded a η of 9.35% with a J_{sc} of 27.78 mAcm^{-2}, a V_{oc} of 552 mV and a *FF* of 0.61. With increasing rGO addition in PEDOT:PSS, the J_{sc} increased from pristine 27.28 mAcm^{-2} to 31.94 mAcm^{-2} for the HSCs with the 2 mg/ml rGO addition, then decreased to 30.41 mAcm^{-2} with further addition of rGO up to 3 mg/ml. Also, the *FF* increased from value of 60.68% (pristine) to 64.75% (2 mg/ml rGO addition), then decreased to 63.75% (3 mg/ml rGO addition). The η enhanced from 9.35% (pristine) to 11.95% (2 mg/ml rGO addition), then decreased to 10.77% (3 mg/ml rGO addition). By the rGO insertion, the R_s decreased from pristine 4.22–3.02 Ωcm^2 (2 mg/ml rGO addition), then increased to 3.49 Ωcm^2 (3 mg/ml rGO addition).

The properties of Si-organic HSCs originated from the heterojunction formed between metal-like polymer PEDOT:PSS and n type Si substrate, and the optical and electrical properties of PEDOT:PSS have an important influence on the device performances. As for the V_{oc} are related to the following Eq. (1) determined by diode qualities [37]:

$$V_{oc} = kT/q\ln(J_{sc}/J_0 + 1) \quad (1)$$

Eq. (1) shows that the V_{oc} of a solar cell mainly depends on the J_{sc} and reverse saturated dark current density (J_0), where k is Boltzmann's constant, T is temperature, and q is charge of an electron. According to the J-V curves in Fig. 6b, it can be seen that J_0 is suppressed significantly by rGO addition due to the suppression of electron recombination at the junction interface, implying the junction property is improved without creating additional defects at the junction interface,leading to a boosted the open-circuit voltage (V_{oc}) and fill factor (*FF*) [38].

Fig. 6c presents the external quantum efficiency (EQE) of fabricated Si-organic HSCs. The EQE improved markedly in the visible and near-infrared region for the fabricated Si-organic HSCs with rGO addition compared to those of without rGO addition. EQE

sometimes referred to also as "incident photon to current conversion efficiency" (IPCE) corresponds to the number of electrons measured as photocurrent in the external circuit divided by the monochromatic photon flux that strikes the cell. It can be described as the product of three components which are the light harvesting efficiency for photons of wavelength λ (LHE), the charge injection efficiency (φ_{inj}) and the charge collection efficiency (η_{coll}) [39]:

$$IPCE = LHE(\lambda).\varphi_{inj}.\eta_{coll} \quad (2)$$

Where LHE is primarily related to the absorption of solar cell materials. Regarding Si-organic HSCs, incident photons can be harvested by Si and then generate electron-hole pairs instead of PEDOT:PSS [16]. From Fig. 6d we can get a conclusion that LHE showed positive impacts in 300–550 nm while negitave influence beyond the 550 nm after rGO addition of the device. In addition, the conductivity of organic film is decided by the carrier mobility and the carrier concentration. According to the Liu, et al. reported that free-carrier absorption in the wavelength of 1000–1100 nm can lead to a lower EQE [16,19]. Whereas, the enhancement of EQE in the infrared region (850–1100 nm) as shown in Fig. 6c implying that improvement of the carrier mobility rather than the carrier concentration. So, the increased carrier mobility contribute to the improved carrier collection efficiency of the device using PEDOT:PSS/rGO composite thin films. Also, it could be deduce that rGO addition has little influence on φ_{inj} for EQE of device. Therefore, from Eq. (2), we can draw a conclusion that the broadband enhancement in EQE from 300 nm to 1100 nm corresponds to the increased carrier collection efficiency and the influence of light harvesting efficiency in the device, owing to the improved electrical conductivity of PEDOT:PSS thin films and the reduced reflectance in the 350–550 nm wavelength by employing rGQ [40].

Fig. 6d is the optical reflectance of Si wafer, PEDOT:PSS/c-Si and PEDOT:PSS(rGO)/c-Si composite thin films. It can be seen that the reflectance of PEDOT:PSS thin films dramatically decreased in comparison with that of planar Si, as previous report that the PEDOT:PSS thin film could serve as an antireflection coating to reduce the reflectance of silicon layer [16]. After rGO addition, the reflectance of PEDOT:PSS thin films reduced in the region of 300–550 nm, while a little improvement beyond the 550 nm can be observed. Mehta, et al. have reported that the graphene overlayer on the polished Si surface can drastically reduce the reflectance value from 88 to 43% to 17–11% in the 300–650 nm wavelength range [41]. So, it can be believed that the rGO in PEDOT:PSS thin films could serve as an antireflection coating to further reduce the reflectance in the 350–550 nm wavelength.

4. Conclusion

Introduction of ultrasonic cell disruptor treatment rGO flakes to PEDOT:PSS thin films as hole transport layer for Si-PEDOT:PSS HSCs has demonstrated to be an efficient and promising means to enhance the solar cells performances. When rGO was added to PEDOT:PSS thin films, the electrical conductivity improved 35%. And the fabricated HSCs with 2 mg/ml rGO addition delivered an overall PCE of 11.95%, about 27.8% increase from 9.35% in pristine HSC, and the short-circuit current density, open-circuit voltage and fill factor were all significantly improved. This enhancement could be due to the fact: (1) the addition of rGO flakes can serve as an antireflection coating to further reduce the reflectance, and (2) the interaction between the conductive rGO flakes and the aromatic structure of PEDOT can provide additional charge transport pathways in hole transport layer and suppress the electron recombination at the junction interface, significantly reduce the sheet resistance of PEDOT:PSS thin films, the series resistance and dark current density of the device, leading improved carrier collection efficiency of the PEDOT:PSS hole transporting layer.

Acknowledgements

This work was supported by the National Natural Science Foundation of China (No. 61376011, 51362026). The authors wish to thank the China Scholarship Council (CSC) for its fellowship assistance.

Appendix A. Supplementary data

Supplementary data associated with this article can be found, in the online version, at http://dx.doi.org/10.1016/j.apsusc.2017.02.193.

References

[1] F. Meillaud, M. Boccard, G. Bugnon, M. Despeisse, S. Hänni, F.J. Haug, J. Persoz, J.W. Schüttauf, M. Stuckelberger, C. Ballif, Recent advances and remaining challenges in thin-film silicon photovoltaic technology, Mater. Today 18 (2015) 378–384.
[2] V.M. Fthenakis, H.C. Kim, Photovoltaics: life-cycle analyses, Sol. Energy 85 (2011) 1609–1628.
[3] L. He, C. Rusli, H. Jiang, D. Wang, Lai, Simple approach of fabricating high efficiency Si nanowire/conductive polymer hybrid solar cells, IEEE Electron Device Lett. 32 (2011) 0741–3106.
[4] P. Yu, C.-Y. Tsai, J.-K. Chang, C.-C. Lai, P.-H. Chen, Y.-C. Lai, P.-T. Tsai, M.-C. Li, H.-T. Pan, Y.-Y. Huang, C.-I. Wu, Y.-L. Chueh, S.-W. Chen, C.-H. Du, S.-F. Horng, H.-F. Meng, 13% efficiency hybrid organic/silicon-nanowire heterojunction solar cell via interface engineering, ACS Nano 8 (2014) 11369–11376.
[5] J. Schmidt, V. Titova, D. Zielke, Organic-silicon heterojunction solar cells: open-circuit voltage potential and stability, Appl. Phys. Lett 103 (2013) 183901.
[6] S. Jäckle, M. Liebhaber, J. Niederhausen, M. Büchele, R. Félix, R.G. Wilks, M. Bär, K. Lips, S. Christiansen, Unveiling the hybrid n-Si/PEDOT:PSS interface, ACS Appl. Mater. Interfaces 8 (2016) 8841–8848.
[7] S. Jäckle, M. Mattiza, M. Liebhaber, G. Brönstrup, M. Rommel, K. Lips, S. Christiansen, Junction formation and current transport mechanisms in hybrid n-Si/PEDOT:PSS solar cells, Sci. Rep. 5 (2015) 13008.
[8] J. Sheng, K. Fan, D. Wang, C. Han, J. Fang, P. Gao, J. Ye, Improvement of the SiOxPassivation layer for high-efficiency Si/PEDOT:PSS heterojunction solar cells, ACS Appl. Mater. Interfaces 6 (2014) 16027–16034.
[9] D. Zielke, C. Niehaves, W. Lövenich, A. Elschner, M. Hörteis, J. Schmidt, Organic-silicon solar cells exceeding 20% efficiency, Energy Proced. 77 (2015) 331–339.
[10] M. Vosgueritchian, D.J. Lipomi, Z. Bao, Highly conductive and transparent PEDOT:PSS films with a fluorosurfactant for stretchable and flexible transparent electrodes, Adv. Funct. Mater. 22 (2012) 421–428.
[11] Y. Zhang, F. Zu, S.-T. Lee, L. Liao, N. Zhao, B. Sun, Heterojunction with organic thin layers on silicon for record efficiency hybrid solar cells, Adv. Energy Mater. 4 (2014) 1300923.
[12] J. Zhang, T. Song, X. Shen, X. Yu, S.-T. Lee, B. Sun, A 12%-efficient upgraded metallurgical grade silicon-organic heterojunction solar cell achieved by a self-purifying process, ACS Nano 8 (2014) 11369–11376.
[13] Z. Ge, L. Xu, Y. Cao, T. Wu, H. Song, Z. Ma, J. Xu, K. Chen, Substantial improvement of short wavelength response in n-SiNW/PEDOT:PSS solar cell, Nanoscale Res. Lett. 10 (2015).
[14] T. Subramani, H.-J. Syu, C.-T. Liu, C.-C. Hsueh, S.-T. Yang, C.-F. Lin, Low-pressure-assisted coating method to improve interface between PEDOT:PSS and silicon nanotips for high-efficiency organic/inorganic hybrid solar cells via solution process, ACS Appl. Mater. Interfaces 8 (2016) 2406–2415.
[15] J.P. Thomas, K.T. Leung, Defect-minimized PEDOT:PSS/Planar-Si solar cell with very high efficiency, Adv. Funct. Mater. 24 (2014) 4978–4985.
[16] Q. Liu, R. Ishikawa, S. Funada, T. Ohki, K. Ueno, H. Shirai, Highly efficient solution-processed poly(3, 4-ethylenedio-xythiophene):poly(styrenesulfonate)/crystalline-silicon heterojunction solar cells with improved light-Induced stability, Adv. Energy Mater. 5 (2015) 1500744.
[17] Y.-S. Kou, S.-T. Yang, S. Thiyagu, C.-T. Liu, J.-W. Wu, C.-F. Lin, Solution-processed carrier selective layers for high efficiency organic/nanostructured-silicon hybrid solar cells, Nanoscale 8 (2016) 5379–5385.
[18] Y.-S. Hsiao, W.-T. Whang, C.-P. Chen, Y.-C. Chen, High-conductivity poly (3, 4-ethylene dioxythiophene):poly(styrene sulfonate) film for use in ITO-free polymer solar cells, J. Mater. Chem. 18 (2008) 5948.
[19] Q. Liu, T. Imamura, T. Hiate, I. Khatri, Z. Tang, R. Ishikawa, K. Ueno, H. Shirai, Optical anisotropy in solvent-modified poly(3,4-ethylenedioxythiophene):poly(styrenesulfonic acid) and its effect on

the photovoltaic performance of crystalline silicon/organic heterojunction solar cells, Appl. Phys. Lett. 102 (2013) 243902.
[20] Q. Liu, M. Ono, Z. Tang, R. Ishikawa, K. Ueno, H. Shirai, Highly efficient crystalline silicon/Zonyl fluorosurfactant-treated organic heterojunction solar cells, Appl. Phys. Lett. 100 (2012) 183901.
[21] D. Li, X. Li, X. Hou, X. Sun, B. Liu, D. He, Building a Ni_3S_2 nanotube array and investigating its application as an electrode for lithium ion batteries, Chem. Commun. 50 (2014) 9361–9364.
[22] T. Qin, B. Liu, Y. Wen, Z. Wang, X. Jiang, Z. Wan, S. Peng, G. Cao, D. He, Freestanding flexible graphene foams@polypyrrole@MnO2electrodes for high-performance supercapacitors, J. Mater. Chem. A 4 (2016) 9196–9203.
[23] Q. Su, S. Pang, V. Alijani, C. Li, X. Feng, K. Müllen, Composites of graphene with large aromatic molecules, Adv. Mater. 21 (2009) 3191–3195.
[24] K. Jo, T. Lee, H.J. Choi, J.H. Park, D.J. Lee, D.W. Lee, B.-S. Kim, Stable aqueous dispersion of reduced graphene nanosheets via non-covalent functionalization with conducting polymers and application in transparent electrodes, Langmuir 27 (2011) 2014–2018.
[25] J. Zhang, X.S. Zhao, Conducting polymers directly coated on reduced graphene oxide sheets as high-performance supercapacitor electrodes, J. Phys. Chem. C 116 (2012) 5420–5426.
[26] X. Wu, F. Li, W. Wu, T. Guo, Flexible organic light emitting diodes based on double-layered graphene/PEDOT:PSS conductive film formed by spray-coating, Vacuum 101 (2014) 53–56.
[27] W. Hong, Y. Xu, G. Lu, C. Li, G. Shi, Transparent graphene/PEDOT–PSS composite films as counter electrodes of dye-sensitized solar cells, Electrochem. Commun. 10 (2008) 1555–1558.
[28] L. Huang, Y. Huang, J. Liang, X. Wan, Y. Chen, Graphene-based conducting inks for direct inkjet printing of flexible conductive patterns and their applications in electric circuits and chemical sensors, Nano Res. 4 (2011) 675–684.
[29] Y. Seekaew, S. Lokavee, D. Phokharatkul, A. Wisitsoraat, T. Kerdcharoen, C. Wongchoosuk, Low-cost and flexible printed graphene–PEDOT:PSS gas sensor for ammonia detection, Org. Electron. 15 (2014) 2971–2981.
[30] Z. Tang, Q. Liu, I. Khatri, R. Ishikawa, K. Ueno, H. Shirai, Optical properties and carrier transport in c-Si/conductive PEDOT:PSS(GO) composite heterojunctions, Phys. Status Solidi (c) 9 (2012) 2075–2078.
[31] J. Ou, J. Wang, S. Liu, B. Mu, J. Ren, H. Wang, S. Yang, Tribology study of reduced graphene oxide sheets on silicon substrate synthesized via covalent assembly, Langmuir 26 (2010) 15830–15836.
[32] D. Yang, A. Velamakanni, G. Bozoklu, S. Park, M. Stoller, R.D. Piner, S. Stankovich, I. Jung, D.A. Field, C.A. Ventrice, R.S. Ruoff, Chemical analysis of graphene oxide films after heat and chemical treatments by X-ray photoelectron and Micro-Raman spectroscopy, Carbon 47 (2009) 145–152.
[33] S. Rattan, P. Singhal, A.L. Verma, Synthesis of PEDOT:PSS (poly(3, 4-ethylenedioxythiophene))/poly(4-styrene sulfonate))/ngps (nanographitic platelets) nanocomposites as chemiresistive sensors for detection of nitroaromatics, Polym. Eng. Sci. (2013), n/a-n/a.
[34] J.P. Thomas, L. Zhao, D. McGillivray, K.T. Leung, High-efficiency hybrid solar cells by nanostructural modification in PEDOT:PSS with co-solvent addition, J. Mater. Chem. A 2 (2014) 2383.
[35] D. Yoo, J. Kim, J.H. Kim, Direct synthesis of highly conductive poly(3,4-ethylenedioxythiophene):poly(4-styrenesulfonate) (PEDOT:PSS)/graphene composites and their applications in energy harvesting systems, Nano Res. 7 (2014) 717–730.
[36] G.H. Kim, D.H. Hwang, S.I. Woo, Thermoelectric properties of nanocomposite thin films prepared with poly(3,4-ethylenedioxythiophene) poly(styrenesulfonate) and graphene, Phys. Chem. Chem. Phys. 14 (2012) 3530.
[37] Y. Liu, Z.-G. Zhang, Z. Xia, J. Zhang, Y. Liu, F. Liang, Y. Li, T. Song, X. Yu, S.-T. Lee, B. Sun, High performance nanostructured silicon–organic quasip–nJunction solar cells via low-temperature deposited hole and electron selective layer, ACS Nano 10 (2016) 704–712.
[38] Q. Liu, I. Khatri, R. Ishikawa, A. Fujimori, K. Ueno, K. Manabe, H. Nishino, H. Shirai, Improved photovoltaic performance of crystalline-Si/organic Schottky junction solar cells using ferroelectric polymers, Appl. Phys. Lett. 103 (2013) 163503.
[39] M. Grätzel, The magic world of nanocrystals, from batteries to solar cells, Curr. Appl. Phys. 6 (2006) e2–e7.
[40] X. Fang, T. Song, R. Liu, B. Sun, Two-dimensional CoS nanosheets used for high-performance organic–inorganic hybrid solar cells, J. Phys. Chem. C 118 (2014) 20238–20245.
[41] R. Kumar, A.K. Sharma, M. Bhatnagar, B.R. Mehta, S. Rath, Antireflection properties of graphene layers on planar and textured silicon surfaces, Nanotechnology 24 (2013) 165402.